

Further Investigation on Model-Independent Probe of Heavy Neutral Higgs Bosons at the LHC Run 2

Yu-Ping Kuang^{1,2,1} Hong-Yu Ren^{1,2} Ling-Hao Xia^{1,3}

¹ *Department of Physics, Tsinghua University, Beijing, 100084, China and*
² *Center for High Energy Physics, Tsinghua University, Beijing, 100084, China*
 (Dated: January 29, 2022)

In our previous paper [1], we provided general effective Higgs interactions for the lightest Higgs boson h (SM-like) and a heavier neutral Higgs boson H based on the effective Lagrangian formulation up to the dim-6 interactions, and then proposed two sensitive processes for probing H . We showed in several examples that the resonance peak of H and its dim-6 effective coupling constants (ECC) can be detected at the LHC Run 2 with reasonable integrated luminosity. In this paper, we further perform a more thorough study of the most sensitive process, $pp \rightarrow VH^* \rightarrow VVV$, on the information about the relations between the $1\sigma, 3\sigma, 5\sigma$ statistical significance and the corresponding ranges of the Higgs ECC for an integrated luminosity of 100 fb^{-1} . These results have two useful applications in the LHC Run 2: (A) realizing the experimental determination of the ECC in the dim-6 interactions if H is found and, (B) obtaining the theoretical exclusion bounds if H is not found. Some alternative processes sensitive for certain ranges of the ECC are also analyzed.

PACS numbers: 14.80.Ec, 12.60.Fr, 12.15.-y

I. INTRODUCTION

After the discovery of the 125 GeV Higgs in 2012 at the CERN LHC [2], the ATLAS and CMS collaborations have measured its couplings to other particles[3][4]. So far, to the present experimental precision, they turn out to be all consistent with the standard model (SM) predictions. However, it does not mean that the SM is the final theory of fundamental interactions since it has several shortcomings, such as unnaturalness[5], triviality[6], vacuum instability[7] and its lack of a suitable dark matter candidate. Searching for new physics beyond the SM is still the main task in the TeV scale particle physics. So far, there is no evidence of the well-known new physics models such as supersymmetry, large extra dimensions, etc.

We know that most new physics models contain several Higgs bosons, and the lightest one may behave as (or very close to) the SM Higgs boson, while the masses of other heavy Higgs are usually in the few hundred GeV to 1 TeV range. Therefore, the discovered 125 GeV Higgs boson may actually be the lightest Higgs boson in a new physics model. So that searching for a heavier Higgs boson may be a feasible way to find the evidence of new physics. Heavy Higgs bosons in several most popular models such as the minimal supersymmetric extension of the standard model (MSSM) and the two-Higgs-doublet model (2HDM) [8] were searched for during the LHC Run 1, but no positive evidence has been found. Therefore, a model-independent probe of the neutral heavy Higgs bosons is a more efficient way of doing it. In our previous paper [1], we provided general effective Higgs interactions for the

lightest Higgs boson h (SM-like) and a heavier neutral Higgs boson H based on the effective Lagrangian formulation up to the dim-6 interactions, and then we proposed two sensitive processes, namely the weak-boson scattering $VV \rightarrow VV$ (WBS) and $pp \rightarrow VH^* \rightarrow VVV$ (VH^*), where $V = W, Z$, for probing H . We showed in several examples that the resonance peak of H and its dim-6 effective coupling constants (ECC) can be detected at the LHC Run 2 with reasonable integrated luminosity. Experimentally, the CMS collaboration performs a more general search, which gives the exclusion limit for a neutral heavy Higgs boson with the SM couplings up to an overall factor C' [9].

In this paper, as in Ref.[1], we consider an arbitrary new physics theory containing more than one Higgs fields Φ_1, Φ_2, \dots without specifying the number of Φ_i and their representations. Their interaction potential $V(\Phi_1, \Phi_2, \dots)$ may, in general, cause mixing between the Higgs fields, and form a set of mass eigenstates. We denote the lightest mass eigenstate by Φ_h , and the second lightest one by Φ_H . The neutral Higgs bosons in Φ_h and Φ_H will be denoted by h and H , respectively. Here we identify h with the discovered 125 GeV Higgs boson.

In the language of effective Lagrangian, we expand the effective interactions up to the dim-6 terms. Since h is identified with the discovered 125 GeV SM-like Higgs boson with vanishing dim-6 interactions. For H , the effective interactions can be expressed by

$$\mathcal{L} = \mathcal{L}^{(4)} + \mathcal{L}^{(6)}. \quad (1)$$

Since Φ_H is a mixture of the original Higgs Fields Φ_1, Φ_2, \dots , the gauge coupling g_H and vacuum expectation value (VEV) v_H of H may be different from the

original coupling g and the VEV v . We define

$$\rho_H \equiv \frac{g_H^2 v_H}{g^2 v} \quad (2)$$

to reflect the mixing effect. the dim-4 term in Eq. (1) can then be expressed as:

$$\begin{aligned} \mathcal{L}_{HWW}^{(4)} &= g M_W \rho_H H W_\mu W^\mu, \\ \mathcal{L}_{HZZ}^{(4)} &= \frac{g M_W \rho_H}{2c^2} H Z_\mu Z^\mu. \end{aligned} \quad (3)$$

where $c \equiv \cos \theta_W$.

The dim-6 interactions between H and gauge bosons can be written through effective Lagrangian as:

$$\mathcal{L}_{HVV}^{(6)} = \sum_n \frac{f_n}{\Lambda^2} \mathcal{O}_n \quad (4)$$

where Λ is the scale under which the effective Lagrangian works. Here we take $\Lambda = 3$ TeV which is consistent with the theoretical argument $\Lambda \sim 4\pi v$ and with the present LHC results on heavy particle searches. \mathcal{O}_n are dim-6 operators composed of H and the $SU(2)_L \times U(1)$ gauge fields with extra derivatives [10–12]. The dim-6 HWW and HZZ interactions relevant to this study are

$$\begin{aligned} \mathcal{L}_{HZZ}^{(6)} &= g_{HZZ}^{(1)} Z_{\mu\nu} Z^\mu \partial^\nu H + g_{HZZ}^{(2)} H Z_{\mu\nu} Z^{\mu\nu} \\ \mathcal{L}_{HWW}^{(6)} &= g_{HWW}^{(1)} (W_{\mu\nu}^+ W^{-\mu} \partial^\nu H + \text{h.c.}) \\ &\quad + g_{HWW}^{(2)} H W_{\mu\nu}^+ W^{-\mu\nu}, \end{aligned} \quad (5)$$

in which

$$\begin{aligned} g_{HZZ}^{(1)} &= g M_W \rho_H \frac{c^2 f_W + s^2 f_B}{2c^2 \Lambda^2}, \\ g_{HZZ}^{(2)} &= -g M_W \rho_H \frac{s^4 f_{BB} + c^4 f_{WW}}{2c^2 \Lambda^2}, \\ g_{HWW}^{(1)} &= g M_W \rho_H \frac{f_W}{2\Lambda^2}, \quad g_{HWW}^{(2)} = -g M_W \rho_H \frac{f_{WW}}{\Lambda^2}, \end{aligned} \quad (6)$$

where $c \equiv \cos \theta_W$, $s \equiv \sin \theta_W$. Because of the smallness of s^2 , Eq. (6) is mainly described by two effective coupling constants (ECC) $\rho_H f_W/\Lambda^2$ and $\rho_H f_{WW}/\Lambda^2$ [1].

In the interactions between H and fermions, the main relevant one is the $H\bar{t}t$ interaction. It has been shown that, up to dim-6 terms, the $H\bar{t}t$ interaction can be expressed as

$$\mathcal{L}_{H\bar{t}t} = y_t^H \bar{t}_L \Phi_H t_R + \text{h.c.} \equiv C_t y_f^{SM} \bar{t}_L \Phi_H t_R + \text{h.c.}, \quad (7)$$

where C_t is a parameter reflecting the deviation from the SM Yukawa coupling constant.

Now we have altogether five parameters, namely the mass of the heavy Higgs boson M_H , the anomalous Yukawa coupling factor C_t , the anomalous gauge coupling constant ρ_H in the dim-4 HVV interaction, and the anomalous coupling constants f_W and f_{WW} in the dim-6 HVV interactions. They characterize the heavy neutral Higgs boson H model-independently. In our study, we

take $M_H = 400$ GeV, 500 GeV, and 800 GeV to represent three ranges of M_H .

In Ref. [1], we pointed out, via several examples, that VH^* and WBS are sensitive processes for discovering H and detecting its ECC $\rho_H f_W/\Lambda^2$ and $\rho_H f_{WW}/\Lambda^2$. In this paper, we shall give a more thorough analysis on the relations between the 1σ , 3σ , 5σ statistical significance and the corresponding ranges of the four ECC for the most sensitive process VH^* for an integrated luminosity of 100 fb^{-1} . If signal of the neutral heavy Higgs boson H is detected at the 3σ (evidence) or 5σ level (discovery) level, this analysis can provide the specific way of realizing the experimental determination of $\rho_H f_W/\Lambda^2$ and $\rho_H f_{WW}/\Lambda^2$. If no signal of H is seen, the 1σ analysis can provide the theoretical exclusion bounds [13] on the ECC. In certain ECC ranges, the conventional on-shell production of H via gluon fusion (GF) and vector-boson fusion (VBF) may also help to discover H . We shall also present the corresponding analysis on these processes.

This paper is organized as follows. First, we give a more detailed study on the exclusion bounds on the ECC from the LHC Run 1 data (EB) and the unitarity bound (UB) from the requirement of unitarity of the S matrix element in Sec. 2. We first consider only the dim-4 interactions, and then, without losing generality, we take into account of the dim-6 interactions by taking certain sample values of C_t and ρ_H to provide the two-dimensional plots on the exclusion bounds in the $\rho_H f_W/\Lambda^2$ - $\rho_H f_{WW}/\Lambda^2$ plane for various values of M_H . In Sec. 3, we provide the analysis on the information about the relation between the 1σ , 3σ , 5σ statistical significance and the ranges of the four ECC for the most sensitive process VH^* at the LHC Run 2 taking account of the present bounds given in Sec. 2. In Section 4, we give the results for the GF and VBF processes. Sec. 4 is a discussion on the exclusion bounds if the signal of H is not seen at the LHC Run 2.

II. EXCLUSION BOUNDS FROM THE LHC RUN 1 DATA AND THE UNITARY BOUND

In Ref. [1], we have studied the exclusion bounds from the requirement of the unitarity of the S matrix elements and from the CMS data on excluding the SM-like Higgs boson with mass from 100 GeV to 1 TeV [14] only for several examples. Now we make a more thorough study of the bounds.

Since the on-shell GF Higgs production process in the LHC Run 1 is not sensitive to dim-6 interactions, we first study the exclusion bound without taking account of the dim-6 interactions. Then there are only two parameters C_t and ρ_H left.

Taking the same approach as in Ref. [1], we calculate the exclusion bound (with vanishing dim-6 ECC) in the C_t - ρ_H plane for the cases of $M_H = 400$ GeV, 500 GeV and 800 GeV. The results are plotted in Fig. 1. The region above each curve is the excluded region.

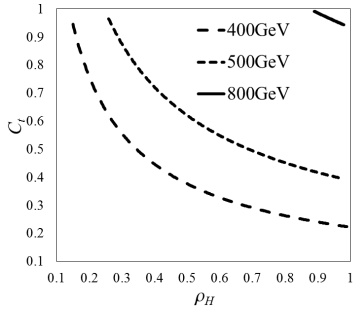


FIG. 1: EB for the cases of $M_H = 400$ GeV (black long dashed), 500 GeV (black short dashed) and 800 GeV (black solid). For each curve, the region above the curve is excluded.

However, as we showed in Ref. [1] that the contribution of the dim-6 interaction with large enough $\rho_H f_W/\Lambda^2$ and/or $\rho_H f_{WW}/\Lambda^2$ may cancel a part of the dim-4 interaction contribution to make H easier to escape from being excluded by EB than what is shown in Fig. 1. Therefore, we should further take into account the contribution of the dim-6 interaction. Now we have to deal with all the four parameters. Of course it is not judicious to plot a four dimensional figure. Note that we are mainly aiming at analyzing the most sensitive process VH^* which is

actually not sensitive to C_t (C_t only affect the total width of H). So we can simply take $C_t = 1$ to represent the Type-I case, and take $C_t = 0.1$ to represent the Type-II case. It is still not easy to read out the exclusion bound quantitatively from a three dimensional plot. So we still need to reduce one parameter. Note that the detection of H from the VH^* process needs a not so small ρ_H . So that the range of ρ_H we are considering is not large. Therefore we can take $\rho_H = 0.2, 0.6$ and 1 to represent three small regions of ρ_H . Then we can plot a two dimensional exclusion bound in the $\rho_H f_W/\Lambda^2$ - $\rho_H f_{WW}/\Lambda^2$ plane which can be quantitatively read. The values of the four parameters we are taking are listed in Table I.

TABLE I: Values of C_t and ρ_H in our study.

Label	A	B	C
Parameter	C_t ρ_H	C_t ρ_H	C_t ρ_H
400GeV I	1 0.2	1 0.6	1 1
500GeV I	1 0.2	1 0.6	1 1
800GeV I	1 0.2	1 0.6	1 1
400GeV II	0.1 0.2	0.1 0.6	0.1 1
500GeV II	0.1 0.2	0.1 0.6	0.1 1
800GeV II	0.1 0.2	0.1 0.6	0.1 1

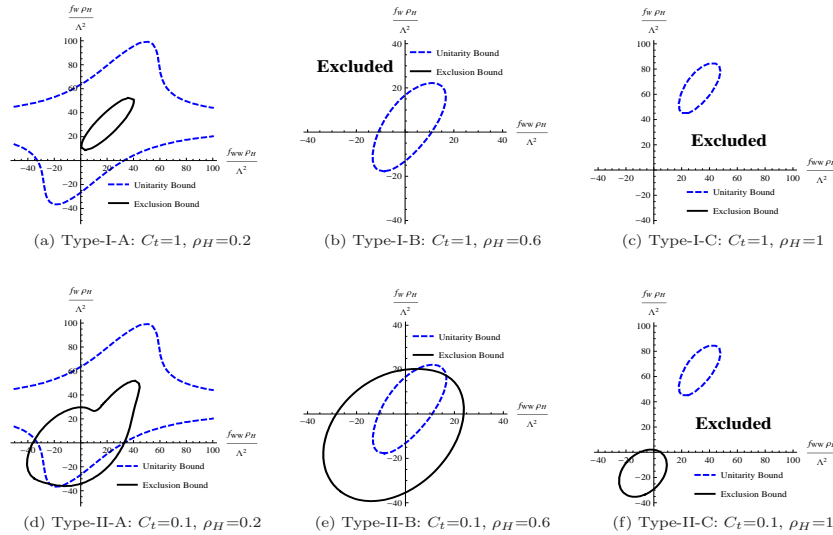


FIG. 2: Exclusion bounds (outside the dark-solid contour) and the unitary bound (outside the blue-dashed contour) for $M_H = 400$ GeV in the $\rho_H f_W/\Lambda^2$ - $\rho_H f_{WW}/\Lambda^2$ plane (in TeV^{-2}).

Taking again the same approach as in Ref. [1], we obtain the exclusion bounds for $M_H = 400$ GeV (Fig. 2),

$M_H = 500$ GeV (Fig. 3), and $M_H = 800$ GeV (Fig. 4). In these figures, the region inside the dark-solid contour

is not excluded, and the blue-dashed curves denote the UB.

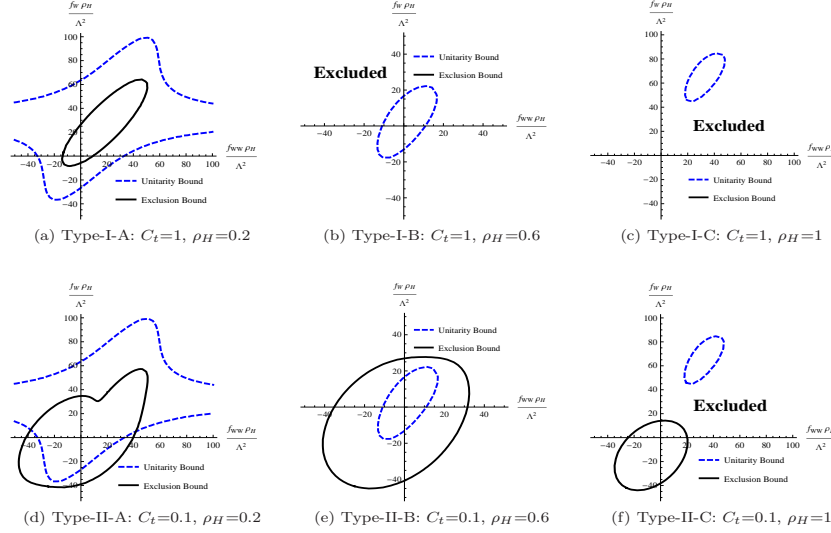


FIG. 3: Exclusion bounds (outside the dark-solid contour) and the unitary bound (outside the blue-dashed contour) for $M_H = 500$ GeV. in the $\rho_H f_W / \Lambda^2$ - $\rho_H f_W W / \Lambda^2$ plane (in TeV^{-2}).

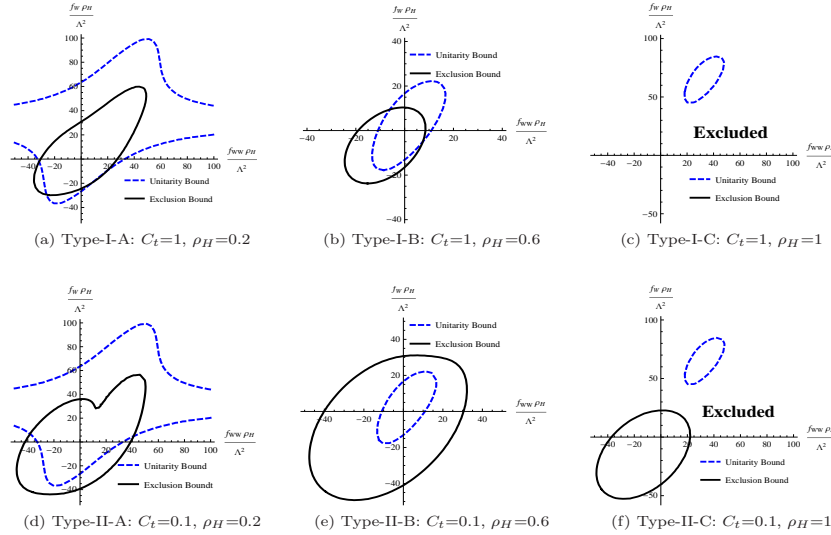


FIG. 4: Exclusion bounds (outside the dark-solid contour) and the unitary bound (outside the blue-dashed contour) for $M_H = 800$ GeV. in the $\rho_H f_W / \Lambda^2$ - $\rho_H f_W W / \Lambda^2$ plane (in TeV^{-2}).

Figure without a dark-solid contour means that the whole region of $\rho_H f_W / \Lambda^2$ and $\rho_H f_W W / \Lambda^2$ is excluded. (e.g., the cases of Type-I-B (Fig. 2(b) and Fig. 3(b)), Type-I-C (Fig. 2 (c) and Fig. 3(c)) for $M_H = 400$ and 500 GeV, and Type-I-C (Fig. 4 (c)) for $M_H = 800$ GeV. In the cases of Type-II-C (Fig. 2 (f), Fig. 3 (f), and Fig. 4 (f)) for $M_H = 400$, 500 and 800 GeV, even

there are dark-solid contours, but they do not overlap with the blue-dashed contours of UB, so that they are also completely excluded. Thus there are only ten parameter sets not being excluded which should be considered in the following sections, namely Type-I-A, Type-II-A, Type-II-B for $M_H = 400$ and 500 GeV (Fig. 2 (a), (d), (e)), Fig. 3 (a), (d), (e)), and Type-I-A, Type-I-B, Type-

II-A, Type-II-B (Fig. 4 (a), (b), (d), (e)) for $M_H = 800$ GeV.

We see that the parameter set $C_t = 1$, $\rho_H = 0.2$ for $M_H = 400$ GeV is in the excluded regions in Fig. 1. However, Fig. 2 (a) shows that there is still a region inside the dark-solid contours not excluded. This means Fig. 1 (neglecting the dim-6 interactions) is too crude, and dim-6 interactions have to be taken into account.

III. ANALYSIS OF VH^* AT LHC RUN 2

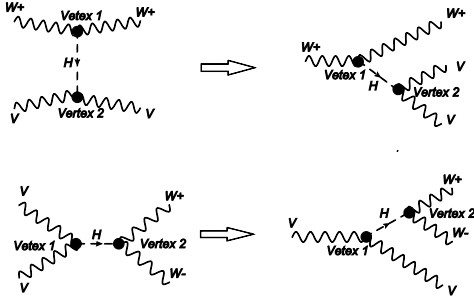


FIG. 5: Feynman diagrams showing the relation between WBS (left) and VH^* (right).

In Ref. [1], we proposed that the semileptonic modes of WBS and VH^* are two sensitive processes for discovering H and measuring its dim-6 interactions at the 14 TeV LHC. The typical Feynman diagrams for WBS and VH^* (having crossing symmetry) with the same ECC and the relation between them are shown in Fig. 5. So their sensitivity of depending on the ECC $\rho_H f_W/\Lambda^2$ and $\rho_H f_{WW}/\Lambda^2$ (in the dim-6 interaction) should be similar. Since the most sensitive process is VH^* , we concentrate on analyzing the VH^* process in this section. We shall

calculate the the ranges of $\rho_H f_W/\Lambda^2$ and $\rho_H f_{WW}/\Lambda^2$ corresponding to the 1σ , 3σ and 5σ statistical significance for the ten allowed parameter sets of C_t and ρ_H mentioned in Sec. 2 for an integrated luminosity of 100 fb^{-1} at the 14 TeV LHC.

We use MadGraph5 [15] interfaced with FeynRules [16] and Pythia6.4 [17] to simulate signals and backgrounds, and take CTEQ6.1 [18] as the parton distribution function (PDF). Delphes3 [19] and fastjet [20] is used to simulate detector acceptance and jet reconstruction. The detector acceptance is set in Table II referring to the design of CMS detector [21].

TABLE II: Detector acceptance according to DELPHES3

	μ	e	jet	photon
$ \eta _{max}$	2.4	2.5	5	2.5
$p_{Tmax}(\text{GeV})$	10	10	20	0.5

We use the Cambridge/Aachen (C/A) algorithm with radius $R=0.8$ [22] to cluster the boosted jets and then apply jet pruning algorithm [23] with parameters $Z_{cut}=0.1$ and $R_{factor_{cut}}=0.5$ on the C/A jets. Then we apply the same cuts as in Ref. [1]. In addition, we only take the events within a small vicinity around the resonance peak of H as what we did in Ref. [1]. The jet pruning algorithm further suppresses the backgrounds.

Let σ_S and σ_B be the cross sections of the signal and background, respectively. For an integrated luminosity \mathcal{L}_{int} , the event numbers N_S and N_B of the signal and background are $N_S = \mathcal{L}_{int}\sigma_S$ and $N_B = \mathcal{L}_{int}\sigma_B$. In the case of $\mathcal{L}_{int} = 100 \text{ fb}^{-1}$ at the 14 TeV LHC, N_S and N_B are large, so that the statistical significance σ_{stat} can be approximately expressed as

$$\sigma_{stat} = \frac{N_S}{\sqrt{N_B}}. \quad (8)$$

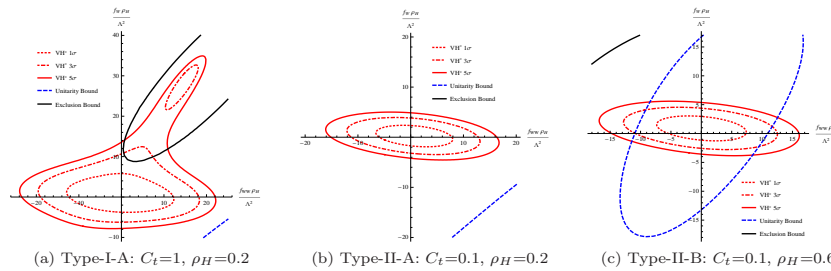


FIG. 6: Contours for 1σ , 3σ and 5σ statistical significance for VH^* on the $\rho_H f_W/\Lambda^2$ - $\rho_H f_{WW}/\Lambda^2$ plane (in TeV^{-2}) for $M_H = 400$ GeV at the 14 TeV LHC with $\mathcal{L}_{int} = 100 \text{ fb}^{-1}$. The EB (dark-solid) and/or UB (blue-dashed) are also shown (or partly shown).

In Fig. 6, Fig. 7, and Fig. 8, we plot the contours

(red-dotted, red-dashed-dotted, and red-solid), in the

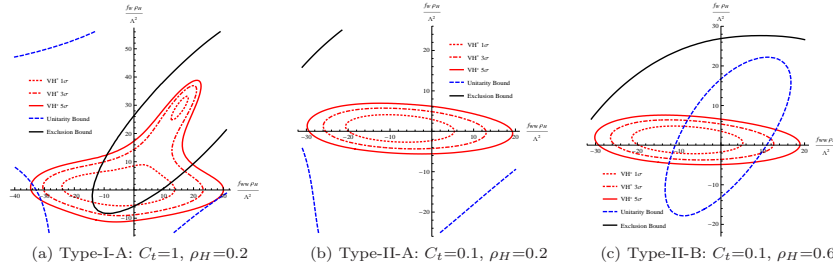


FIG. 7: Contours for 1σ , 3σ and 5σ statistical significance for VH^* on the $\rho_H f_W/\Lambda^2$ - $\rho_H f_{WW}/\Lambda^2$ plane (in TeV^{-2}) for $M_H = 500$ GeV at the 14 TeV LHC with $\mathcal{L}_{\text{int}} = 100 \text{ fb}^{-1}$. The EB (dark-solid) and/or UB (blue-dashed) are also shown (or partly shown).

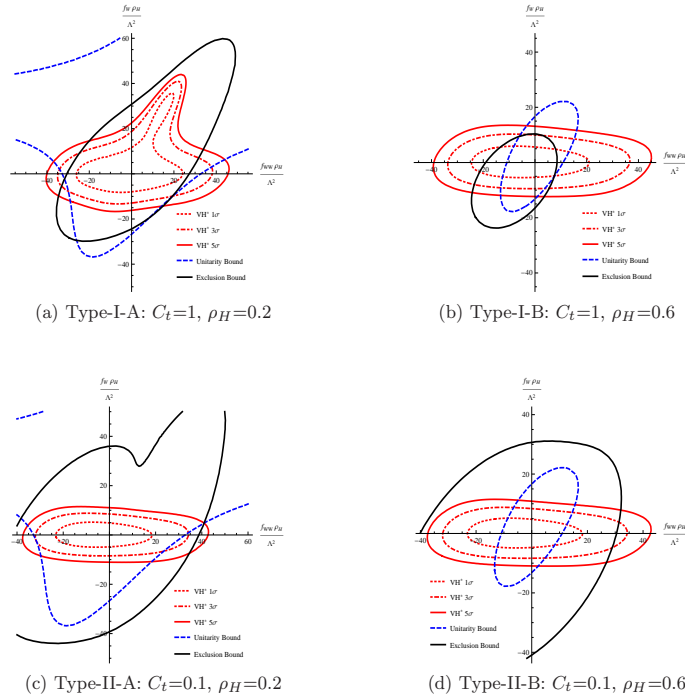


FIG. 8: Contours for 1σ , 3σ and 5σ statistical significance for VH^* on the $\rho_H f_W/\Lambda^2$ - $\rho_H f_{WW}/\Lambda^2$ plane (in TeV^{-2}) for $M_H = 800$ GeV at the 14 TeV LHC with $\mathcal{L}_{\text{int}} = 100 \text{ fb}^{-1}$. The EB (dark-solid) and/or UB (blue-dashed) are also shown (or partly shown).

$\rho_H f_W/\Lambda^2$ - $\rho_H f_{WW}/\Lambda^2$ plane, corresponding to the statistical significance of 1σ (margin), 3σ (evidence) and 5σ (discovery) for the process VH^* with $M_H = 400, 500$, and 800 GeV, respectively. In these figures, we also plot (or partly plot) the EB (dark-solid) and/or the UB (blue-dashed) given in Sec. 2 to show the actual allowed regions. The ten figures in Fig. 6, Fig. 7, and Fig. 8 are for the ten sets of C_t and ρ_H mentioned in Sec. 2.

we see that, in most cases, EB and UB put nontrivial constraints on the red contours. Only some parts of the red contours inside the allowed regions set by the EB and/or UB are actually allowed, while the parts outside the allowed regions are excluded. The only exception is the case of Type-II-A for $M_H = 400$ GeV whose red contours are so small that they are completely well within

the allowed region.

In the following, we discuss two useful applications of these results.

(A) Experimental determination of $\rho_H f_W/\Lambda^2$ and $\rho_H f_{WW}/\Lambda^2$ of H

In Ref. [1], we pointed out that, after the discovery of the resonance peak of H , one can further measure four distributions, namely the $p_T(\text{leptons})$ -, the $p_T(J_1)$ -, the $\Delta R(\ell^+, J_1)$ -, and the $\Delta R(J_1, J_2)$ -distribution, to determine values of $\rho_H f_W/\Lambda^2$ and $\rho_H f_{WW}/\Lambda^2$ of this H (cf. Sec. VIII of Ref. [1]). Now we can see the specific way of realizing it from Fig. 6, Fig. 7, and Fig. 8. Taking the 5σ discovery of H in the case of Type-II-B for $M_H = 500$ GeV (Fig. 7 (c)) as an example, the allowed values

of $\rho_H f_W/\Lambda^2$ and $\rho_H f_{WW}/\Lambda^2$ lie on two segments of the red-solid contour inside the UB allowed region. Thus we can determine the values $\rho_H f_W/\Lambda^2$ and $\rho_H f_{WW}/\Lambda^2$ by adjusting the values on these two segments in the theoretical distributions to fit the experimentally measured distributions. Since these two segments are not long, the best fit values may be easily obtained by iteration. The so determined values of $\rho_H f_W/\Lambda^2$ and $\rho_H f_{WW}/\Lambda^2$ serve as a new powerful high energy criterion for discriminating new physics models. Only models whose predicted $\rho_H f_W/\Lambda^2$ and $\rho_H f_{WW}/\Lambda^2$ are consistent with the experimentally determined values can survive as candidates of the correct new physics models reflecting the nature. All models whose predicted $\rho_H f_W/\Lambda^2$ and $\rho_H f_{WW}/\Lambda^2$ are not consistent with the experimentally determined values will be ruled out.

(B) Theoretical exclusion bounds if H is not discovered at LHC Run 2

In this paper, we take into account only the statistical error, and leave the study of the systematic error to experimentalists. In this sense, the 1σ contours for the ten possible parameter sets (cf. Sec. 2) shown in Figs. 6, 7, and 8 play an important role. For each set of C_t and ρ_H , the regions inside the 1σ contour means that the signal is immersed in the statistical fluctuation, i.e., it cannot be detected. Thus, theoretically, if the resonance peak is not found at the 14 TeV LHC, the 1σ contours provide the strongest theoretical exclusion bound on $\rho_H f_W/\Lambda^2$ and $\rho_H f_{WW}/\Lambda^2$ for each set of C_t and ρ_H , i.e., the values of $\rho_H f_W/\Lambda^2$ and $\rho_H f_{WW}/\Lambda^2$ outside the 1σ contours are excluded. Note that in Fig. 6 (a) the 1σ contour is completely in the excluded region. In this case, the whole allowed region is excluded.

IV. ANALYSIS OF GF AND VBF AT LHC RUN 2

On-shell Higgs productions via GF and VBF are traditional processes in the discovery and measurement of

the 125 GeV Higgs boson h at the LHC Run 1. The most accurate measurement comes from the decay mode $h \rightarrow ZZ \rightarrow 4\ell$. In Ref. [1], we pointed out that the dim-6 interactions are suppressed by a factor k^2/Λ^2 relative to the dim-4 interactions, where k is a typical momentum scale (from the extra derivatives in the dim-6 interactions) appearing in the dim-6 interaction, and it is of the order of the momentum of the Higgs boson. In on-shell Higgs productions of the heavy Higgs boson H , $k^2 \sim M_H^2$. Taking $M_H = 500$ GeV with $\Lambda = 3$ TeV as an example, $k^2/\Lambda^2 \sim (500/3000)^2 = 0.03$. This means that the dim-6 interactions only contribute about 3% of the total contribution. So that it is hard to measure the effect of the dim-6 interactions in on-shell Higgs productions. This is the reason why we concentrate our study on the VH^* process. However, in certain regions of the ECC, on-shell productions of H via GF and VBF may still help for discovering H . So, for completeness, we analyze these two processes in this section.

The signals and backgrounds for the GF and VBF processes in the LHC Run 1 have been analyzed in Ref. [24]. Here we take the same approach as in Sec. 2. For the signals, we take the production cross sections and branching ratios given by the LHC Higgs Cross Section Working Group [25] and rescale their distributions. For the main background of GF, $pp \rightarrow ZZ \rightarrow 4\ell$, we rescale it with the K-factor given in Ref. [26]. We take the anti- k_T algorithm with radius $R=0.5$ [27] to cluster jets and refer to the research of the CMS collaboration on 4ℓ mode of Higgs decay [24] to apply cuts in this section. The events in which the final four leptons can reconstruct the mass of H are selected for both the signal and the background processes.

Since the dim-4 interaction dominates in these two on-shell H production processes, we first analyze it neglecting the dim-6 interactions. The 1σ , 3σ and 5σ contours with vanishing dim-6 ECC are plotted in Fig. 9.

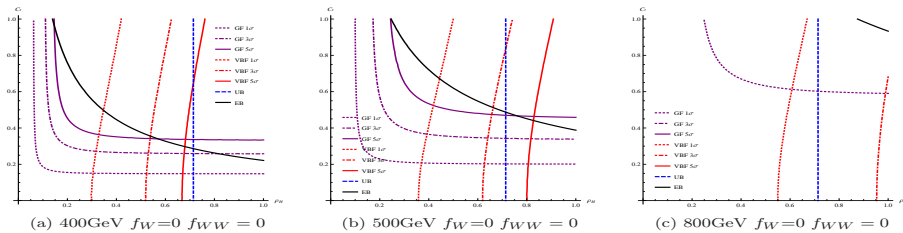


FIG. 9: The 1σ (dotted), 3σ (dashed-dotted) and 5σ (solid) contours of the GF (purple) and VBF (red) processes for H with vanishing dim-6 ECC at the 14 TeV LHC with $\mathcal{L}_{\text{int}} = 100 \text{ fb}^{-1}$. The EB (dark-solid, from Fig. 1) and UB (blue-dotted) are also shown.

We see from Fig. 9 that GF is sensitive for discovering H when C_t and ρ_H are both not so small. However, as we see from Fig. 9, quite a large portion of this region has already been excluded by EB. The VBF process is sensi-

tive when ρ_H is large, but UB excludes the 5σ discovery for $M_H > 500$ GeV, and allows a very narrow region for 5σ discovery only for $M_H = 400$ GeV.

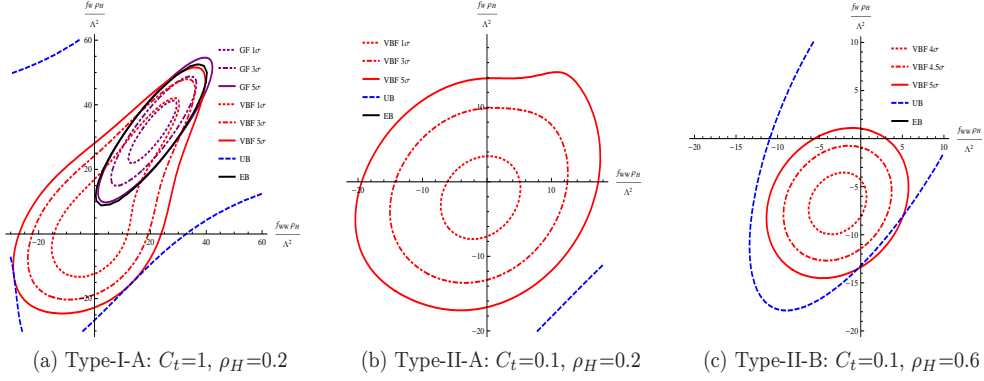


FIG. 10: 1σ , 3σ and 5σ contours for GF (purple-dotted, purple-dashed-dotted, and purple-solid) and VBF (red-dotted, red-dashed-dotted, and red-solid) in the $\rho_H f_W / \Lambda^2$ - $\rho_H f_{WW} / \Lambda^2$ plane (in TeV^{-2}) for $M_H = 400$ GeV at the 14 TeV LHC with $\mathcal{L}_{\text{int}} = 100 \text{ fb}^{-1}$. Except in (a), the tiny contours for GF are ignored.

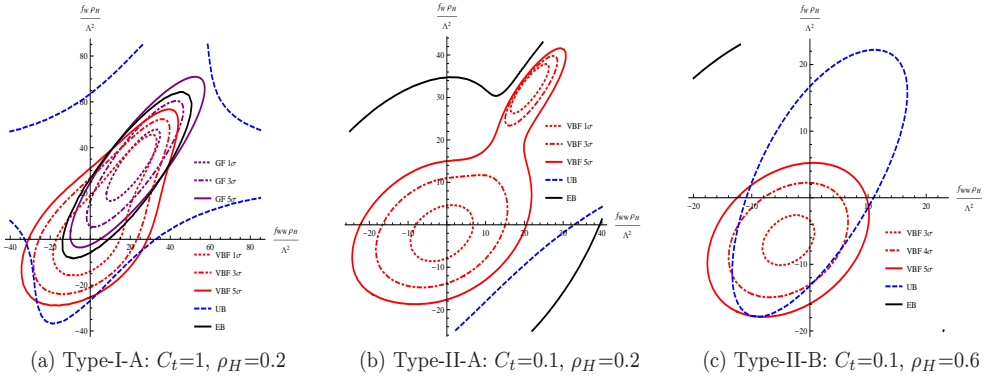


FIG. 11: 1σ , 3σ and 5σ contours for GF (purple-dotted, purple-dashed-dotted, and purple-solid) and VBF (red-dotted, red-dashed-dotted, and red-solid) in the $\rho_H f_W / \Lambda^2$ - $\rho_H f_{WW} / \Lambda^2$ plane (in TeV^{-2}) for $M_H = 500$ GeV at the 14 TeV LHC with $\mathcal{L}_{\text{int}} = 100 \text{ fb}^{-1}$. Except in (a), the tiny contours for GF are ignored.

Next we analyze the general case including the dim-6 interactions. The 1σ , 3σ and 5σ contours for GF (purple) and VBF (red) together with the EB (dark-solid) and UB (blue-dashed) constraints for $M_H = 400, 500$, and 800 GeV are plotted in Fig. 10, 11 and 12, respectively for the ten sets of C_t and ρ_H mentioned in Sec. 2.

We see that GF can help to discover H only in the case of Type-I-A with very narrow available parameter ranges, and can hardly discover H in all other cases. VBF can help to discover H in more cases except Type-I-B for $M_H = 800$ GeV, but the available parameter ranges are

all quite small.

Comparing Fig. 10 (a) with Fig. 6 (a), we see that the 1σ contour for GF and VBF are larger than that for VH^* . So that if H is not discovered, VH^* still gives the strongest exclusion bound.

We also see that the density of the contours for VH^* process is much larger than that for GF and VBF. This means that VH^* is much more sensitive to the variation of $\rho_H f_W / \Lambda^2$ and $\rho_H f_{WW} / \Lambda^2$. This is why we only suggest measuring $\rho_H f_W / \Lambda^2$ and $\rho_H f_{WW} / \Lambda^2$ via VH^* .

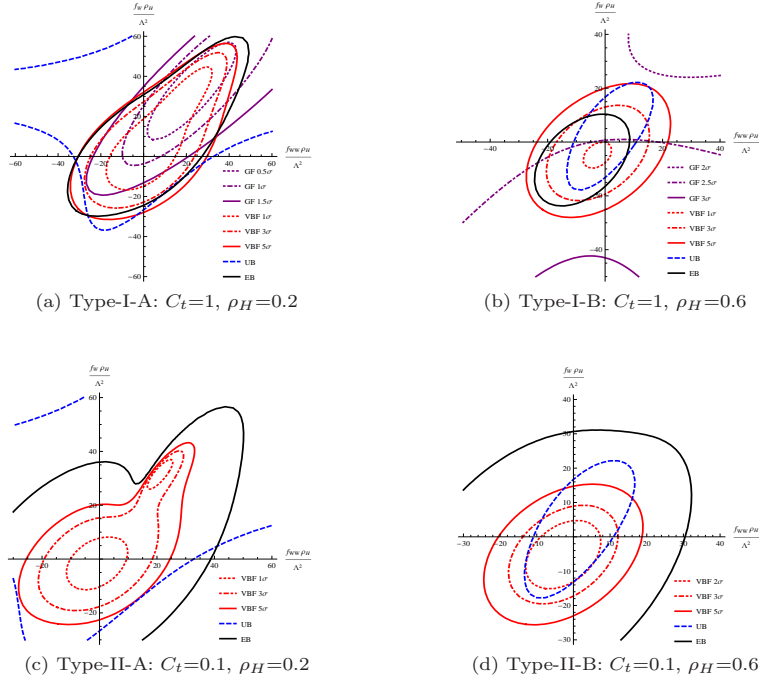


FIG. 12: 1σ , 3σ and 5σ contours for GF (purple-dotted, purple-dashed-dotted, and purple-solid) and VBF (red-dotted, red-dashed-dotted, and red-solid) in the $\rho_H f_W/\Lambda^2$ - $\rho_H f_{WW}/\Lambda^2$ plane (in TeV^{-2}) for $M_H = 800$ GeV at the 14 TeV LHC with $\mathcal{L}_{\text{int}} = 100 \text{ fb}^{-1}$. Except in (a) and (b), the tiny contours for GF are ignored.

V. SUMMARY

In this paper, we extend the study in Ref. [1] to a more thorough analysis of EB from the LHC Run 1 data, the UB, and the relations between the statistical significance of 1σ , 3σ , 5σ and the ranges of the ECC in the general effective interactions related to the heavy neutral Higgs boson H . These results are very useful in the Run 2 of the LHC for realizing the experimental determination of $\rho_H f_W/\Lambda^2$ and $\rho_H f_{WW}/\Lambda^2$ if H is discovered, and setting the exclusion bounds on the ECC if H is not found.

We take the same formulation of the effective interactions related to the heavy neutral Higgs boson H as in Ref. [1], which contains five parameters, namely the heavy Higgs mass M_H , the anomalous $Ht\bar{t}$ Yukawa coupling factor C_t , the anomalous gauge coupling constant ρ_H in the dim-4 HVV interactions, and the anomalous gauge coupling constants $\rho_H f_W/\Lambda^2$ and $\rho_H f_{WW}/\Lambda^2$ in the dim-6 HVV interactions. We take $M_H = 400$ GeV, 500 GeV, and 800 GeV to represent three mass ranges of M_H in this study.

It has been pointed out that, at the 14 TeV LHC, the most sensitive processes for discovering H and measuring its $\rho_H f_W/\Lambda^2$ and $\rho_H f_{WW}/\Lambda^2$ is $pp \rightarrow VH^* \rightarrow VVV$ (VH^*). So we concentrate on analyzing the process VH^* in this paper. Since VH^* is not sensitive to the variation of C_t , we just take two values of C_t , namely $C_t = 1$ and $C_t = 0.2$ to represent the two types of anomalous

Yukawa interactions, Type-I and Type-II, respectively. In addition, the process VH^* is detectable only if the HVV interactions are not so weak (the probe of heavy Higgs bosons with very weak HVV interactions (gauge-phobic or nearly gauge-phobic) is given in Ref. [28]), so we consider a not so large range of ρ_H , namely $0.2 < \rho_H < 1$, and divide it to three parts. We take $\rho_H = 0.2$, 0.6 and 1 to represent these three parts. This parameter setting of C_t and ρ_H is shown in Tab. I.

We first gave a more thorough study of the EB from the LHC Run 1 data, and the UB from the requirement of the unitarity of the S matrix elements in Sec. 2 for the parameter sets given in Tab. I. This already gives quite strong constraints on the ECC, and we shall see it plays an important role in the analysis of the VH^* in Sec. 3.

Sec. 3 is the main part of our analysis. We calculated the contours for the statistical significance of 1σ (margin), 3σ (evidence), and 5σ (discovery) with the integrated luminosity $\mathcal{L}_{\text{int}} = 100 \text{ fb}^{-1}$ for the process VH^* at the 14 TeV LHC. The results are plotted in Figs. 6, 7, and 8. These results has two useful applications in the Run 2 of the LHC: (A) realizing the experimental determination of $\rho_H f_W/\Lambda^2$ and $\rho_H f_{WW}/\Lambda^2$ which provides a new high energy criterion for discriminating new physics models, i.e., *Only models whose predicted $\rho_H f_W/\Lambda^2$ and $\rho_H f_{WW}/\Lambda^2$ are consistent with the experimentally determined values can survive as candidates of the correct new physics models reflecting the nature.*, (B) Setting the exclusion bounds on the ECC from the 1σ contours if H

is not found at the LHC Run 2. These are important extensions of the study in Ref. [1].

Finally, for completeness, we also analyzed the traditional processes of on-shell Higgs productions via GF and VBF in Sec. 4. the results are shown in Figs. 9, 10, 11, and 12. First of all, we showed that on-shell Higgs productions via GF and VBF can hardly give contribution to the experimental determination of $\rho_H f_W/\Lambda^2$ and $\rho_H f_{WW}/\Lambda^2$. Then from Figs. 9, 10, 11, and 12 we see that: (i) GF can help to discover H only in the case of Type-I-A with very narrow available parameter ranges, and can hardly discover H in all other cases; (ii) VBF can help to discover H in more cases except Type-I-B for $M_H = 800$ GeV, but the available parameter ranges are all quite small; (iii) if H is not found at the LHC Run 2 experiments, the exclusion bounds on ECC from GF and VBF are significantly weaker than those from VH^* .

In a word, we conclude that VH^* is the best pro-

cess for discovering H and measuring its $\rho_H f_W/\Lambda^2$ and $\rho_H f_{WW}/\Lambda^2$ at Run 2 of the LHC.

Acknowledgments

We are grateful to Guo-Ming Chen for valuable discussions. We would like to thank Tsinghua National Laboratory for Information Science and Technology for providing their computing facility. This work is supported by the National Natural Science Foundation of China under the grant numbers 11135003 and 11275102.

-
- [1] Yu-Ping Kuang, Hong-Yu Ren, and Ling-Hao Xia, *Phys. Rev. D* **90** (2014) 115002.
 - [2] G. Aad *et al.*, (ATLAS Collaboration), *Phys. Lett. B* **716** (2012) 1; W. Adam *et al.*, (CMS Collaboration), *Phys. Lett. B* **716** (2012) 30.
 - [3] ATLAS Collaboration, *ATLAS-CONF-2014-09* (2014).
 - [4] CMS collaboration, *CMS-PAS-HIG-14-009* (2014).
 - [5] L. Susskind, *Phys. Rev. D* **20** (1979) 2619.
 - [6] R. Dashen and H. Neuberger, *Phys. Rev. Lett.* **50** (1983) 1897.
 - [7] G. Degrandi, Giuseppe, et al., *JHEP* **1208** (2012) 098.
 - [8] G. Aad *et al.* (ATLAS Collaboration), *Phys. Rev. D* **89** (2014) 032002.
 - [9] CMS collaboration, *CMS-PAS-HIG-13-031* (2015).
 - [10] K. Hagiwara, S. Ishihara, R. Szalapski, and D. Zeppenfeld, *Phys. Rev. D* **48** (1993) 2182.
 - [11] W. Buchmüller and D. Wyler, *Nucl. Phys. B* **268**, 621 (1986).
 - [12] For a review, see M.C. Gonzalez-Garcia, *Int. J. Mod. Phys. A* **14**, 3121 (1999).
 - [13] This theoretical exclusion bound is not the same as the experimental 95% C.L. exclusion bound which depends on the data and the total error (including the systematic error). The experimental 95% C.L. exclusion bound can only be obtained when the measurement is done, and can only be given by the experimentalists.
 - [14] CMS Collaboration, Report No. *CMS-PAS-HIG-13-002* (unpublished).
 - [15] J. Alwall, M. Herquet, F. Maltoni, O. Mattelaer, and T. Stelzer, *JHEP* **1106** (2011) 128.
 - [16] A. Alloul, N. D. Christensen, C. Degrande, C. Duhr and B. Fuks, *Comput. Phys. Commun.* **185** (2014).
 - [17] T. Sjostrand, S. Mrenna, and P. Skands, *JHEP* **0605** (2006) 026.
 - [18] D. Stump, J. Huston, J. Pumplin, W.-K. Tung, H.-L. Lai, S. Kuhlmann, and J. F. Owens, *JHEP* **0310** (2003) 046.
 - [19] J. Favereau, C. Delaere, P. Demin, A. Giammanco, V. Lemaitre, A. Mertens, and M. Selvaggi, *JHEP* **1402** (2014) 057.
 - [20] M. Cacciari, G. P. Salam and G. Soyez, *Euro Phys. J. C* **72** (2012) 1896.
 - [21] S. Chatrchyan, et al. (CMS collaboration), *J. Instrumen.* **3** (2008) S08004.
 - [22] Y. L. Dokshitzer, G. D. Leder, S. Moretti, and B. R. Webber, *JHEP* **9708** (1007) 001.
 - [23] S. D. Ellis, C. K. Vermilion and J. R. Walsh, *Phys. Rev. D* **80** (2009) 051501; *Phys. Rev. D* **81** (2010) 094023.
 - [24] CMS collaboration, *CMS-PAS-HIG-13-002* (2013).
 - [25] S. Dittmaier *et al.*, (LHC Higgs Cross Section Working Group), *CERN-2011-002* (2011); S. Dittmaier *et al.*, (LHC Higgs Cross Section Working Group), *CERN-2012-002* (2012).
 - [26] T. Binoth, N. Kauer and P. Mertsch, *arXiv:0807.0024* [hep-ph].
 - [27] M. Cacciari, G. P. Salam and G. Soyez, *JHEP* **0804**, (2008) 063.
 - [28] Y.-P. Kuang and L.-H. Xia, *Phys. Lett. B* **747** (2015) 193–199.